BIOCHEMISTRY
including biophysical chemistry & molecular biology

Article

pubs.acs.org/biochemistry

Mutational Analysis of Sulfite Reductase Hemoprotein Reveals the Mechanism for Coordinated Electron and Proton Transfer

Kyle W. Smith and M. Elizabeth Stroupe*

Department of Biological Science and Institute of Molecular Biophysics, Florida State University, Tallahassee, Florida 32306-4380, United States

Supporting Information

ABSTRACT: Sulfite reductase catalyzes the six-electron reduction of sulfite to sulfide. The active site, found in the hemoprotein subunit (SiRHP), sits on the distal face of a negatively charged porphyrinoid called siroheme whose central iron atom is coupled to a proximal Fe_4S_4 cluster. Four positively charged amino acids are positioned around the active site cavity. Together, these two arginines (R83 and R153) and two lysines (K215 and K217) mitigate the negative charge on the siroheme macrocycle. They also serve as a cage around the distally bound anion that tightens when substrate binds and an active site loop clamps down. Structures of native SiRHP point to these amino acids as being important, but their specific roles are ill-defined. Here, we have altered those four active site amino acids and one amino acid on the flexible loop (N149) to probe their roles in SiRHP activity. None of these positively charged residues is required for electron transfer, but only R83S and N149W variants can produce a fully reduced product. By measuring the electrons used per unit of reduced sulfur released, we show that K215, R153, and K217 are responsible for intermediate and late proton transfers, whereas N149 and R153 play a role in the structure of the flexible loop that controls anion binding and release. R83 is primarily responsible for siroheme binding. Together, the activities and structures of these variants reveal specific roles for each in anion binding and in coupled proton transfer that facilitates electron transfer.

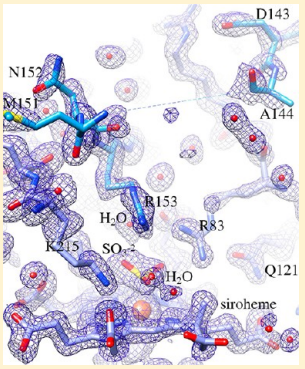

Sulfur is one of the essential elements in nature, found in its reduced form (S^{2-}) in amino acids cysteine and methionine, vitamins thiamine and biotin, and the peptide antioxidant glutathione. Environmentally, sulfur is also found in its elemental form (S) and as inorganic sulfate (SO_4^{2-}). In *Escherichia coli*, activated sulfate is first reduced to sulfite (SO_3^{2-}). Next, sulfite reductase (SiR) reduces SO_3^{2-} by six electrons to make sulfide (S^{2-}).[1] The six-electron reduction of SO_3^{2-} to S^{2-} and that of nitrite (NO_2^-) to ammonia (NH_3) are the only examples of a single-step six-electron reduction found in nature, so understanding the catalytic mechanism of SiR is a key aspect of understanding the bio−geo cycle of sulfur in the environment.

Sulfur reduction is found in two pathways in nature as part of the general sulfur cycle. Some bacteria, archae, fungi, and plants generate bioavailable S^{2-} for incorporation into sulfur-containing biomolecules.[1] In contrast, a broad niche of sulfate-dependent anaerobic organisms can respire using sulfur rather than oxygen as the terminal electron acceptor in anaerobic respiration.[2] The redox active metalloenzyme SiR is central to both pathways. Two isoforms of SiR, called assimilatory (SiRHP) or dissimilatory (DSR), use a similar protein architecture and unique cofactor assembly to catalyze the six-electron redox reaction (Figure 1).[3−7] In both, a central cleft at the junction of three domains houses an Fe_4S_4 cluster covalently bound to the iron of a porphyrinoid called siroheme.[8] Together, these cofactors pass electrons to the distally bound substrate.

At the center of the catalytic mechanism is siroheme, an ancient, iron-containing macrocyclic porphyrinoid.[9] Unlike its distant cousin, heme, siroheme has two unconjugated pyrroline rings in addition to two that are fully conjugated.[10] The flexibility afforded by the unconjugated rings allows a significant saddle-shape bend across the macrocycle that, in turn, allows tight association of the distally bound anion (Figure 1B).[3,11] Siroheme also has negatively charged acetyl and proponyl groups at the corners of the macrocycle that distinguish it from other protoporphyrin-derived hemes. Charge−charge interactions between these functional groups and positively charged amino acid side chains from the central siroheme-binding cleft are integral to cofactor and substrate binding.[3−7]

Three elements of particular importance contribute to catalysis: anion binding and/or release through interactions with the cationic cage of amino acids, structural rearrangement of a flexible loop around the active site, and coupled electron and proton transfer to substrate. Static X-ray crystallographic structures give hints about how individual amino acids contribute to each element, but the dynamic interplay among these three elements is what makes this enzyme unique. Characterizing the effect of altering amino acids that are central to anion binding, the flexible loop, and proton transfer is one

Received: July 16, 2012
Revised: November 15, 2012
Published: November 15, 2012

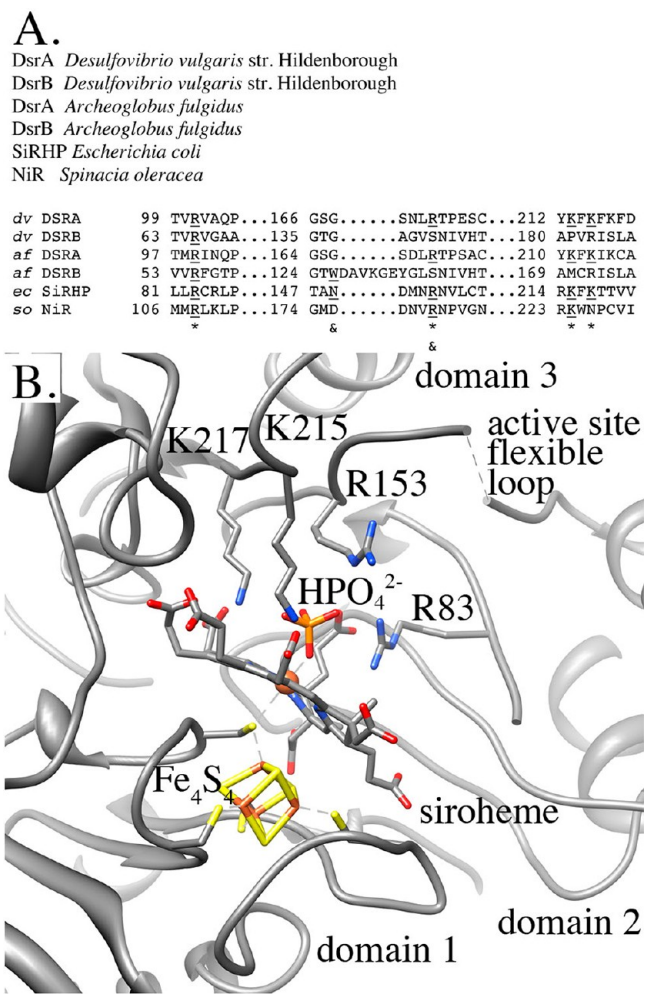

Figure 1. (A) Sequence alignment of important active site residues in SiRHP from *E. coli* and *Spinacia oleracea* and DSR from *Desulfovibrio vulgaris* str. Hildenborough and *Archeoglobus fulgidus*. Amino acids important for substrate binding are marked with an asterisk, and those from the flexible active site loop are marked with an ampersand. (B) Ribbon diagram of assimilatory SiRHP (PDB entry 1AOP[3]). The active site is in a cleft at the center of three domains, marked by the presence of a cage of cationic residues and a flexible loop that is disordered in the resting state of the enzyme. All figures were rendered in UCSF Chimera.[29]

way to address the remaining questions about how all aspects of SiRHP work together.

Anion binding in the active site is determined by the shape of the ligand, which determines how it interacts with this cage formed by positively charged side chains that project into the active site.[11,12] In the enzyme's resting, oxidized state, a phosphate molecule occupies the active site and coordinates the siroheme through one of its oxygen atoms. The phosphate is larger than the substrate SO_3^{2-} or NO_2^- and inhibits the clamping down of a flexible loop containing residues 144−153; residues 146−148 are missing from the X-ray crystal structure.[3] Upon reduction of the siroheme and Fe_4S_4 cluster, the phosphate molecule diffuses out of the active site.[13] SO_3^{2-} binds the siroheme through its central sulfur atom and pulls in that flexible loop to tightly organize an active site that is primed for coupled proton and electron transfer. In total, six protons combine with the substrate's three oxygens to yield three water molecules. The metallic cofactors act in concert with this high proton gradient in a proposed "push−pull" mechanism to move electrons, akin to that seen in other dehydrogenases and oxygenases.[11,14]

One proposed mechanism for electron transfer in SiR involves three steps of two electrons coupled to substrate dehydration, facilitated by protons donated by the enzyme.[11,12] Partially reduced intermediates of SO_3^{2-} are not observed in assimilatory SiRHP, though, so this "three-steps-of-two" mechanism remains untested. With limiting electrons, a stable two-electron reduced SO_2^{2-}-bound species is formed, but the absence of an EPR signal associated with the complex precludes identification of the exact nature of the intermediate.[15] Upon oxidation of the adduct, that complex is reversible, and with further reducing equivalents, the complex turns over to completion. Further, a three-electron-reduced intermediate (ferroheme-NO) is trapped when SiRHP is provided with its alternative substrate, NO_2^-, that leaves open the possibility that single-electron transfers can occur.[15] Proton transfer is an equally important aspect of SiRHP's mechanism. Despite suggestive cocrystal structures of SiRHP and DSR with anions of varying geometries, the source of the protons and the order of the dehydration reactions to remove the anion oxygens remain unknown.[11,12]

To test the catalytic role of R83, R153, K215, and K217 as well as that of the flexible active site loop consisting of residues 144−153, we have made and characterized the following single-site variants: R83S, R153S, K215S, K217S, and N149W. R153S and N149W variants were generated to mimic a structural siroheme binding site in *Archaeoglobus fulgidus* dissimilatory sulfite reductase (*af*DSR),[5] whereas R83S, K215S, and K217S variants were generated to further probe the enzyme mechanism. We show that each variant exhibits unique activity that isolates the roles of these amino acids in anion binding, proton transfer, and product release. R83, K215, and K217 are important for anion binding because phosphate does not bind to variants harboring serine in any of those positions. All of the variants can catalyze electron transfer, but only R83S and N149W variants produce fully reduced product. On the basis of the activity and stoichiometry of electron transfer to product release for each of these variants, we propose a detailed mechanism for proton transfer that helps pull electrons onto the substrate.

EXPERIMENTAL PROCEDURES

Protein Expression and Purification. *E. coli* assimilatory *cysI* and *Salmonella typhimurium cysG* were subcloned as a bicistronic gene into the pBAD-A (Invitrogen) plasmid where *cysI* was fused with the coding sequence for an N-terminal six-histidine tag (called pBAD-his-*cysIG*). *cysI* encodes SiRHP and *cysG* siroheme synthase, whose coexpression is required for overexpressing active SiRHP.[16] Variants were generated by altering the appropriate *cysI* codons in this background using the QuikChange (Stratagene) method for site-directed mutagenesis. The following primers and their reverse complements were used to template the alterations (IDT): R83S (CGCGATGCTGTTGAGCTGCCGTCTG), R153S (CGCTAACGACATGAACAGCAACGTAC), K215S (CCTGCCGCGTAGCTTCAAAACCACGGTA), K217S (CCTGCCGCGTAAATTCAGCACCACGGTA), and N149W (CTGGCGACCGCTTGGGACATGAACCG). Alterations were confirmed with DNA sequencing (Operon).

Enzymes were expressed in the LMG194 strain of *E. coli* (Invitrogen) grown to midlog phase in Luria-Bertani (LB)

Table 1. Data Collection and Refinement Statistics

	N149W	N149W-SO_3^{2-}	R153S
	Data Collection		
refined resolution range (Å)	22.8−1.56	33.1−1.56	43.9−2.1
space group	$P2_12_12_1$	$P2_12_12_1$	$P2_12_12_1$
unit cell dimensions (Å)	66.3 × 76.2 × 81.5	66.4 × 76.2 × 81.4	67.6 × 77.0 × 86.9
completeness	97.6 (91.8)	95.5 (80.0)	88.5 (44.0)
R_{merge} (%)	5.5 (21.4)	11.0 (48.7)	14.4 (44.2)
$I/\sigma(I)$	54.8 (9.1)	28.7 (2.3)	21.7 (2.4)
redundancy	8.8 (7.2)	11.2 (4.2)	5.8 (2.8)
Wilson *B* value (Å^2)	11.6	12.1	30.3
	Refinement		
no. of atoms	4204	4169	3975
no. of reflections	57743 (1992)	56173 (2025)	23260 (2000)
$R_{working}$ (%)	15.3	15.4	18.1
R_{free} (%)	18.4	18.6	23.5
root-mean-square deviation for bonds (Å)	0.008	0.007	0.01
root-mean-square deviation for angles (deg)	1.65	1.56	1.32
average *B* value	16.3	16.3	35.5
B value for protein	14.4	23.6	33.4
B value for waters	27.9	44.4	36.6
B value for ligands	12.3	14.8	31.5

medium and induced with 0.05% arabinose. Cells were resuspended in 10 mM KP_i (pH 7.8) and lysed using the French press method.

Lysate clarified with centrifugation at 16000*g* was then passed over a Ni-charged immobilized metal affinity column (GE Healthcare) and eluted across a gradient of imidazole from 20 to 500 mM in 65 mM KP_i (pH 7.8) and 300 mM NaCl. SiRHP-containing fractions were identified by its unique red color and SDS−PAGE analysis, then pooled, dialyzed in 50 mM KP_i (pH 7.8), concentrated, and passed over an S300 Sephadex size exclusion column (GE Healthcare) in 50 mM KP_i (pH 7.8) and 300 mM NaCl, where it fractionated at the expected position for a monomer of about 64000 Da. All SiRHP mutants required further purification using ion exchange chromatography. Protein was dialyzed into 50 mM KP_i (pH 6) and then passed over an SP Sepharose cation exchange column (GE Healthcare). Fractions containing SiRHP were then dialyzed into 50 mM KP_i (pH 8) and passed over a Q Sepharose anion exchange column (GE Healthcare). Purified samples were dialyzed into 50 mM KP_i (pH 7.8) before being further analyzed. All chromatography was performed on an AKTA Purifier (GE Healthcare).

The protein concentration was assayed using the bichinoic acid (BCA) method (Pierce) to obtain an extinction coefficient at 280 nm for each variant. This extinction coefficient was subsequently used for all protein concentration calculations. The siroheme absorbance was measured on a Nanodrop spectrophotometer and the concentration calculated using the published extinction coefficient at 386 nm (6.56 mM^{-1} mm^{-1}).[17]

Complementation Assays. To qualitatively assess each variant's ability to complement wild-type activity, a *cysI* knockout strain of *E. coli*[18] was transformed with native, point mutant, and empty pBAD-his-*cysIG* and grown to full density in LB medium. Cultures were harvested with centrifugation and washed three times in water before being resuspended in water to equal cell density. Serial dilutions of the cultures were spotted on M9 minimal medium[19] containing only an inorganic sulfate source and supplemented with 0.05% arabinose; growth was assessed after 48 h at 37 °C.

Crystal Growth, Anaerobic SO_3^{2-} Soak, Acquisition of X-ray Data, and Refinement of Data. Crystals of N194W and R153S were grown from protein that had been cleaved with trypsin for 30 min. For R153S, 16 mg/mL enzyme was mixed to a final concentration of 65 mM KP_i (pH 7.8) and 22% PEG MW 8000 and nucleated by microseeding and vapor diffusion with native seeds followed by reseeding with R153S crystals. N149W crystals nucleated independently at 3 mg/mL in vapor diffusion drops against 65 mM KP_i and 12% PEG MW 8000, but microseeding was used to enhance crystal formation.

N149W crystals were introduced into an anaerobic glovebox working under a N_2 atmosphere fitted with a stereomicroscope for crystal work (mBRAUN). After overnight equilibration in the anaerobic chamber, crystals were transferred to degassed drops containing 50% PEG MW 8000 and 50 mM SO_3^{2-} in 65 mM Na-HEPES buffer (pH 7.8). Soaks were performed for 36 h, and crystals were frozen in liquid nitrogen while they were still in the glovebox and transferred to the atmosphere in cryo-cooled APS-style cryo-pucks.

For the collection of aerobic data, single crystals were mixed with 50% PEG MW 8000 and frozen in liquid nitrogen before being mounted in pucks for the collection of synchrotron data. Data for N149W and the N149W soak were collected at 22-BM, and data for R153S were collected at 22-ID, both part of the SER-CAT line at Argonne National Laboratory (Argonne, IL). Both experiments were performed at 0.1 nm X-ray radiation on a MAR-300 CCD (MarResearch). Data were integrated and reduced with HKL2000.[20]

In the case of the N149W variant (both oxidized and soaked), 360° of data with an angular increment of 1° were collected (Table 1). In the case of the R153S variant, crystals were significantly smaller than the N149W crystals despite repeated attempts at improving crystal growth (changing the temperature of crystal growth, additives, and crystal seeding conditions). As a result, the crystals were significantly more sensitive to radiation damage, and so data were collected

dx.doi.org/10.1021/bi300947a | *Biochemistry* 2012, 51, 9857−9868

through only 200° of data collection with a 1° angular increment (Table 1).

Phases were determined in PHENIX[21] with molecular replacement against a native SiRHP structure (PDB entry 1AOP[3]). For N149W and the N149W soak, amino acids 144–151 were removed from the search model to reduce model bias. For R153S, reside 153 was replaced with an alanine. For both search models, all water and cofactor molecules were removed. The subsequent structures were refined and the variant-containing loops rebuilt through iterative rounds of manual fitting in Coot[22] and energy minimization, occupancy, and *B* factor refinement in PHENIX (Table 1).

The default restraints that define siroheme in PHENIX are based on the planar siroheme seen in the DSR structures.[4−7] Initial refinements with these default restraints resulted in significant difference density around the siroheme. To enforce the bowed siroheme found in assimilatory SiRHP[3] and visualized in the density seen in all structures we analyzed (Figure S3 of the Supporting Information), additional restraints on the torsion angles of the two unconjugated pyrroline rings were used during refinement to ensure that the siroheme retained its bowed conformation (Table S2 of the Supporting Information).

SiRHP Activity. Solutions of 100 mM KP_i (pH 7.9), 0.5 N HCl, and 0.5 M EDTA (pH 8.0) were thoroughly degassed by bubbling nitrogen gas into the solutions for 30 min followed by three freeze–thaw cycles in a dry ice/acetone slurry under vacuum and a N_2 atmosphere. The septum-sealed flasks were moved immediately to the glovebox antechamber. All solids [Cr(II)Cl_2 (Sigma-Aldrich), sodium sulfite (Na_2SO_3), methyl viologen (MV^+; Sigma-Aldrich), and hydroxylamine (NH_2OH)] were introduced into the glovebox as solids, and anaerobic solutions were prepared as described below.

Cr(II)EDTA was generated by dissolving Cr(II)Cl_2 in 0.5 N HCl to a concentration of 0.5 M;[13] 700 μL of 0.5 M EDTA and 300 μL of 0.5 M Cr(II)Cl_2 were mixed to produce 0.15 M Cr(II)EDTA. This mixture immediately becomes pale blue, which turns to a dark purple over several hours. The Cr(II)EDTA mixture was incubated overnight at room temperature to reach a stable solution.

The following triplicate reaction mixtures for the assays were prepared anaerobically in 1 cm path length, septum-sealed cuvettes as follows: 100 mM KP_i (pH 7.9), 1 mM substrate (either SO_3^{2-} or NH_2OH), 100 μM MV, and 150 μM Cr(II)EDTA. Reactions were initiated via injection of 1 μL of SiRHP by gastight syringe into the reaction mixture. The reduction of the acceptor (either SO_3^{2-} or NH_2OH) was monitored by following the oxidation of MV^+ at 604 nm (ε = 13000 M^{-1} cm^{-1} [23]) on a Varian Cary 50 Bio spectrophotometer operating the "Enzyme Kinetics" software package. MV^+ has a characteristic blue color that goes to clear as it releases electrons to the enzyme.

Specific activities for electron transfer were determined by calculating the change in MV^+ over time using the calculated siroheme concentration from its absorbance at 386 nm. Reactions with SO_3^{2-} were repeated at 0.5 mM acceptor to verify that the reactions were saturating for all variants. SO_3^{2-} binds the native enzyme 2 orders of magnitude stronger than NH_2OH, so 1 mM NH_2OH is well beyond saturation for all variants.[17]

Sulfide Production. To assess the formation of the product, reduced sulfur equivalents were measured using a methylene blue-based colorometric assay[24] with slight modification. Reduced sulfur [either sulfide (S^{2-}) or dithionite ($S_2O_4^{2-}$), in the presence of MV^+ and CrII(EDTA) but not sulfite (SO_3^{2-}), trithionite ($S_2O_6^{2-}$), or thiosulfate ($S_2O_3^{2-}$)] causes the stoichiometric formation of methylene blue from *N*,*N*-dimethyl-*p*-phenylenediamine (DPD) and acidified $FeCl_3$. The concentration of methylene blue formed can then be measured spectrophotometrically at 650 nm using an extinction coefficient of 19000 M^{-1} cm^{-1}.[24]

First, anaerobic reactions were set up as described for the specific activity measurements. Electron equivalents were determined by calculating the decrease in the amount of MV^+ at 604 nm. At completion of the reduction reaction, the anaerobic reaction mixtures were exposed to air by injecting a 1 mL syringe of air into sealed cuvettes to quench remaining reductant, while preserving the liberated H_2S gas. Next, DPD and $FeCl_3$·HCl were injected into the same sealed cuvette using a gastight syringe. The ratio of electrons to reduced sulfur was determined by comparing molar equivalents from each part of the assay.

Phosphate Binding. To assess the binding of HPO_4^{2-} and SO_3^{2-} to SiRHP variants, all proteins were extensively dialyzed against 100 mM HEPES buffer (pH 7.8). Concentrations were determined on the basis of the absorbance at A_{280} using the calculated extinction coefficient from the BCA measurements and then normalized so each variant contained equivalent amounts of siroheme-bound enzyme, with the wild-type enzyme at 0.14 mg/mL, N149W at 0.19 mg/mL, R83S at 2.1 mg/mL, R153S at 0.15 mg/mL, K215S at 0.21 mg/mL, and K217S at 0.42 mg/mL. Next, the enzymes were mixed with 200 mM $K_2H^{32}PO_4$ (Perkin-Elmer) and divided into two aliquots; 500 mM Na_2SO_3 was added to one and an equivalent volume of buffer to the other. Both remained at room temperature overnight. Ten microliters of each was loaded onto a 4–20% Tris-glycine gel (Bio-Rad) and run in Tris-glycine buffer at 120 V for 2 h. The gel was exposed to a phosphoscreen overnight at 20 °C. The phosphoscreen was scanned on a STORM scanner (GE Biosciences).

RESULTS

SiRHP Variant Purification and Spectroscopic Analysis. Variants in substrate binding residues (Figure 1) were made in pBAD-his-*cysIG*. Recombinantly expressed SiRHP requires coexpression of siroheme synthase to make active enzyme;[16] however, even with this coexpression, the variants show siroheme binding defects (Table 2).

Complementation Assays. The wild type and N149W variant fully complement the *cysI*-knockout strain of *E. coli*. All others (R83S, R153S, K217S, and K215S) showed no growth above background (Figure 2).

Table 2. Characterization of the Wild Type and Point Variants

	siroheme occupancy	SO_3^{2-} V_{max} (MV^+ min^{-1} siroheme^{-1})	NH_2OH V_{max} (MV^+ min^{-1} siroheme^{-1})	[oxidized MV^+]/[reduced sulfur]
wild type	1	1320 ± 70	2870 ± 710	6.5 ± 0.7
N149W	0.7	2630 ± 390	5120 ± 170	6.2 ± 0.3
R83S	0.06	784 ± 80	13300 ± 3200	6.2 ± 1.4
R153S	0.9	240 ± 18	9030 ± 1860	4.0 ± 0.8
K217S	0.3	35.8 ± 5.5	6680 ± 380	5.4 ± 0.7
K215S	0.7	14.6 ± 0.5	20.6 ± 3.5	3.3 ± 0.6

dx.doi.org/10.1021/bi300947a | *Biochemistry* 2012, 51, 9857–9868

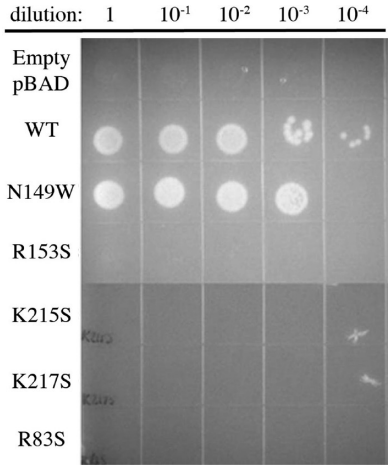

Figure 2. Complementation of *cysI*$^-$ by transformation with the SiRHP gene harboring point mutations on M9 minimal medium supplemented with arabinose for the induction of gene expression. Each row represents a different variant, whereas each column is a 1:10 serial dilution of the original culture, washed and resuspended in water to the same cell density.

X-ray Analysis of the N149W Variant Bound to HPO_4^{2-} and SO_3^{2-}. The N-terminal most residues (L81−R83) and flexible active site loop (D143−N152) are spatially close in SiRHP (Figure 1B) and are structurally coupled to the state of the active site.[3,11,13] In all SiRHP structures, this region of the structure has high *B* factors (more than twice the average *B* factor, regardless of the state of the active site) and amino acids 146−148 are not represented in the wild-type model of the HPO_4^{2-}-bound enzyme (Figure 1B).[3,11,13] Not surprisingly, the X-ray crystallographic structure of the HPO_4^{2-}-bound N149W variant reveals changes to the flexible active site loop, which contains amino acid 149, and to its N-terminal most amino acids (Figure 3A). Despite high *B* factors (40−60 Å^2), the backbone of each amino acid in the loop (residues 144−152) can be traced in the oxidized N149W structure, showing that residues 147−150 form a turn that leads into helix 2 with HPO_4^{2-} bound to the siroheme (Figure 3A).

Subtle differences in the position of the N-terminal amino acids are evident in conjunction with the added detail that is present in the active site loop. Specifically, residues 81−83 adopt a split path. In one, the N-terminal most L81 is not resolved but L82b and R83b adopt a position similar to that in the wild-type enzyme. In the other, a single water molecule bridges the carbonyl of L145 with the backbone carbonyl of L81a and amide of R83a (Figure 3A). This alternative conformation of the N-terminus is further stabilized by a long hydrogen bond between T147's hydroxyl and the backbone carbonyl of L81a, allowing hydrophobic stacking of T147's methyl group and the L81 side chain. Together, these interactions reposition the N-terminal most residues ∼5 Å closer to the active site loop relative to their position in the wild-type structure.

This new position for residues 81−83 is stabilized by a hydrogen bond that forms between the carboxyl of L82a and Nε of Q121, allowed because Q121's side chain has rotated ∼86° around its χ_1 bond relative to where it is in the wild-type structure. In doing so, Q121 no longer makes a water-mediated hydrogen bond with a siroheme proponyl group, seen in the wild-type structure. With the repositioning of those N-terminal amino acids stabilized by Q121, the side chain of R83 flips over. R83 Nη is now free to make a hydrogen bond with Q121 Oε (Figure 3A). Throughout, R83 maintains its interactions with the siroheme-bound phosphate, but the nitrogens involved in the new interaction seen in the alternative conformation are Nη and Nε rather than the two Nη atoms (Figure 3A).

Binding of SO_3^{2-} to the N149W variant results in the same flipping of R153 that facilitates tighter interactions between its

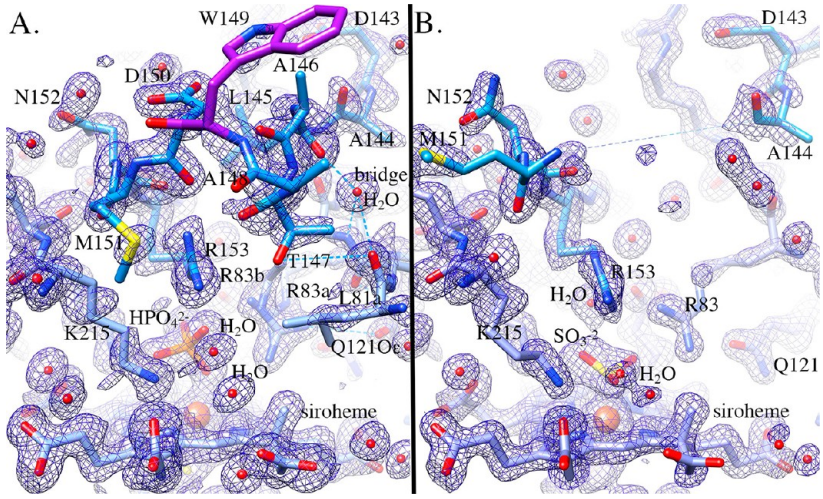

Figure 3. Active site loop in the N149W variant that is visible in the HPO_4^{2-}-bound structure but disordered in the SO_3^{2-}-bound structure. (A) SigmaA-weighted $2F_o - F_c$ electron density[25] contoured at 1σ (blue cages) shows the path of amino acids 144−152 (light blue), including the W149 alteration (purple). Side chains are visible for some, but not all, of the amino acids. The tetrahedral shape of the bound HPO_4^{2-} (orange) and the characteristic bow of the siroheme (light blue) are clear at 1.6 Å resolution. The multiple positions of R83 (R83a and R83b) can also be visualized, with the position of L81−R83a stabilized by the bridging water molecule (red sphere). (B) SigmaA-weighted $2F_o - F_c$ electron density[25] contoured at 1σ (blue cages) shows that anaerobically and in the absence of excess HPO_4^{2-}, SO_3^{2-} (yellow) binds to the N149W siroheme iron (blue bonds and orange sphere) through its central sulfur atom, as it does in the wild-type enzyme. R153 also flips over, mimicking its action in the wild-type enzyme. Even at this contour level, however, no density is evident for amino acids 145−150, showing that the active site loop is unable to coalesce in this variant. Two water molecules (red spheres) are in the same position as they are in the wild-type enzyme.

dx.doi.org/10.1021/bi300947a | *Biochemistry* 2012, 51, 9857−9868

side chain and the bound substrate in the wild-type enzyme (Figure 3B). Whereas the remaining loop residues coalesce around the active site in the wild-type enzyme, those residues become completely disordered in the N149W variant when SO_3^{2-} binds (Figure 3B). Any attempt to model those residues resulted in an increase in R_{free} and strong positive $F_o - F_c$ difference electron density. Additionally, there was no electron density for amino acids 81 and 82, suggesting that the additional freedom of the active site loops extends to the N-terminus. Q121 remains as it is in the wild-type enzyme. The absence of density for those loop residues in the SO_3^{2-}-bound N149W variant is in contrast to the HPO_4^{2-}-bound structure, although they are of comparable resolution (Table 1).

X-ray Analysis of the R153S Variant. The structure of the R153S variant further highlights the relationship between the positively charged active site residues and the flexible loop around the active site. With the shorter side chain at position 153, the active site loop can coalesce around the bound HPO_4^{2-}, as it does when SO_3^{2-} is bound to the siroheme of the wild-type enzyme (Figure 4).[11] S153 rotates away from the

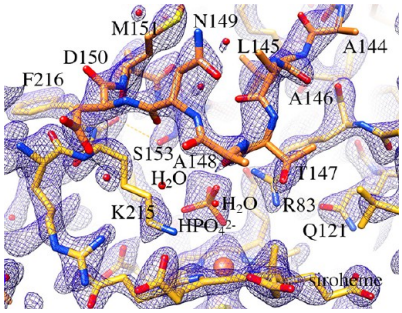

Figure 4. SigmaA-weighted $2F_o - F_c$ density[25] contoured at 1.5σ (blue cages) shows the active site loop containing amino acids 144–151 (orange) are positioned in the clamped position, akin to that in the SO_3^{2-}-bound wild-type enzyme. The ordered solvent molecules (red spheres) are less-well ordered on the basis of their weak electron density and high *B* factors. The nontetrahedrally shaped density around the HPO_4^{2-} and those atom's relatively high *B* factor suggest the anion is weakly bound to the siroheme iron (yellow bonds and orange sphere).

active site so that it forms a hydrogen bond with the carbonyl of F216. The resulting cavity allows amino acids 144–152 to form the turn that links the end of α-helix 2 to β-strand 5. The density for the backbone of these amino acids is well-resolved (Figure 4), but as with all SiRHP structures, the *B* factors are relatively high for this loop (40–60 Å^2).

Evidence of ordered water molecules and anions in the active site is mixed. Additional 4σ SigmaA-weighted $F_o - F_c$ difference density[25] is present when the active site waters are omitted, and the R_{free} is lower when they are included. On the other hand, the resulting SigmaA-weighted $2F_o - F_c$ density[25] is weak (Figure 4), suggesting that the solvent-filled cavity is quite fluid in the presence of the short side chain. Modeled water molecules with high *B* factors (~50 Å^2) were included to accommodate the difference map and reduce R_{free}. Likewise, the distally bound HPO_4^{2-} is less well-defined than it is in the wild-type or N149W variant structures. This is, in part, due to the lower resolution of the R153S variant structure compared to the resolution of the other two. The refined *B* factor is also higher (~40 Å^2, compared to ~11 Å^2 in the structure of the N149W variant).

Attempts To Crystallize the Remaining Variants. Despite attempts to crystallize the remaining variants (R83S, K215S, and K217S), we were unable to produce diffraction-quality crystals. Two of the variants (R83S and K217S) show low siroheme occupancy (Table 2) and variable CD spectra (Figure S2 of the Supporting Information), suggesting that the structures would not likely represent the active, cofactor-bound form of the enzyme. The third (K215S) resulted only in showers of crystals obtained by microseeding from crystals generated from the other variants, remaining recalcitrant to large crystal growth despite our best efforts.

Activity Assay. Specific activities of each variant for electron transfer in the presence of SO_3^{2-} as the acceptor were determined in MV^+ per minute per siroheme based on the change in MV^+ concentration over time (Table 2). N149W is approximately twice as active as the wild-type enzyme, whereas R83S is ~60% as active. R153S is only ~20% as active. K215S and K217S are minimally active. Similar experiments were performed using hydroxylamine (NH_2OH) as the acceptor, showing that with the smaller, partially reduced anion all of the variant-containing enzymes except K215S are more active than the wild-type protein (Table 2).

Sulfide Production. The sulfide detection revealed that, as expected, the wild type and N149W variant both reduce the SO_3^{2-} substrate fully by six electrons (Table 2). Surprisingly, R83S also completes the full six-electron reduction despite its inability to complement the *cysI*$^-$-deficient strain in the absence of reduced sulfur (Table 2 and Figure 2). R153S, although almost 60% as active as the wild type in the transfer of electrons to SO_3^{2-}, reduces the substrate by only 4 reducing equivalents. K217S is active in reducing SO_3^{2-} but releases only 5 equivalents of reduced sulfur. K215S, which shows only trace activity in the transfer of electrons to SO_3^{2-}, reduces the substrate by 3 reducing equivalents.

Phosphate Binding. Only the wild-type enzyme exhibits HPO_4^{2-} binding that is outcompeted by sulfite binding to the oxidized enzyme (Figure 5). N149W and R153S both show

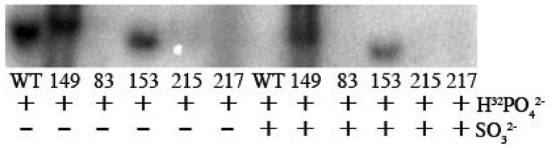

Figure 5. Native gel electrophoresis shows $^{32}PO_4^{2-}$ and SO_3^{2-} binding to the wild type and point variants. All $K_2H^{32}PO_4$ is at 200 μM, and when present, Na_2SO_3 is at 500 μM.

that although HPO_4^{2-} binds to the oxidized active site, it is not completely competed off the siroheme by SO_3^{2-}. R83S, K215S, and K217S show minimal HPO_4^{2-} binding.

DISCUSSION

Here, we have used mutational analysis, enzyme assays, and X-ray structure determination to reveal a detailed mechanism for SiRHP in which six single electrons and protons are sequentially passed to the evolving substrate. SiRHP is proposed to work through a coupled push–pull mechanism whereby electrons are pushed from the redox active cofactors to the substrate while a high proton concentration, donated by the distal cage of lysines and arginines, pulls charge to the substrate (Figure 1A).[11] Next, proton transfer catalyzes reductive cleavage of the S–O bond followed by water release. R83,

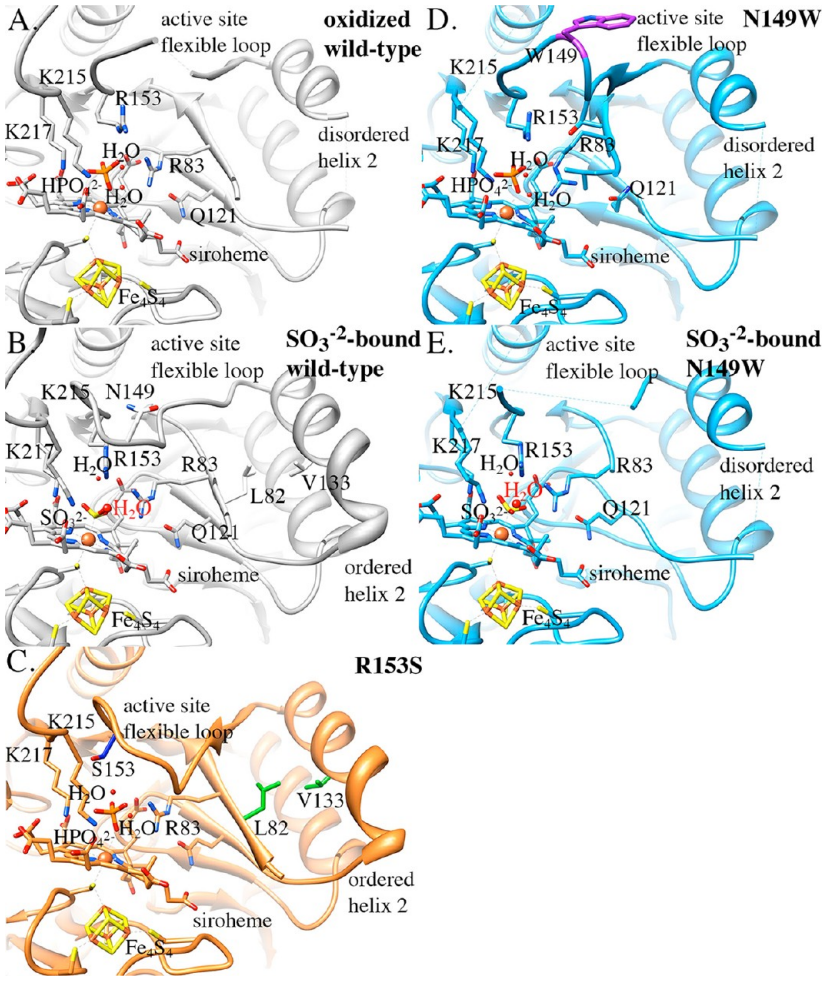

Figure 6. A comparison of the wild-type enzyme (gray ribbons and bonds) with and without SO_3^{2-} (A and B) with the R153S variant (orange ribbons and bonds) (C) and the N149W variant (blue ribbons and bonds) with and without SO_3^{2-} (D and E) and they show structural themes that relate to the enzyme function. (A) The active site flexible loop and helix 2 are disordered in the resting wild-type enzyme. (B) The active site flexible loop clamps over a flipped R153, pulling in the N-terminus of helix 2 when SO_3^{2-} (yellow) binds the siroheme. (C) The R153S variant mimics the SO_3^{2-} bound enzyme in that the active site loop, bearing S153 (blue) is closed and helix 2 is ordered, but HPO_4^{2-} remains loosely bound to the siroheme iron. (D) The active site loop containing W149 (purple) is open but helix 2 is disordered in the N149W variant. (E) When SO_3^{2-} binds the N149W variant, R153 flips as it does in (B) but neither the active site loop nor helix 2 is ordered.

R153, K215, and K217 are highly conserved across different SiRs (Figure 1A), are structurally important for substrate binding (Figure 6), and have been proposed to be proton sources, whether directly or indirectly through structural water molecules.[3−7] Additionally, X-ray crystallographic structures of SiR bound to different anions (HPO_4^{2-}, HSO_3^-, NO_2^-, NO, CO, CN, and SO)[11,12] suggest a mechanism for electron and proton transfer wherein the anion's oxygens are removed sequentially, starting with the protonated O3 of SO_3^{2-}, followed by O1, and finally O2. Without functional data, however, the exact source of protons at each step is not clear solely from the structural data, because each oxygen binds at least two potential donors.

Our results support the proposed push−pull mechanism because when true individual proton donors are removed by altering their side chain to a serine (in this case, R153, K215, and K217 but not R83), the six-electron transfer does not go to completion (Table 2). Rather, the enzyme performs the early stages of the reaction until it stalls at the missing proton source. Naturally, any variation in the active site of an enzyme could affect the native mechanism by fundamentally altering the chemistry performed by the enzyme. We anticipate that if this were the case in SiRHP, then all of the active site variants would show full complementation (i.e., release fully reduced product) because water molecules would be able to rescue any missing proton source. Our choice to replace the arginine/lysine side chains with a serine (rather than an alanine, for example) left open this experimental result. Clearly, this is not the case (Figure 2).

Further, in this way, K215, R153, and K217 are identified as intermediate and late sources of protons, implicating solvent molecules as being responsible for the earliest protons (Table 2). R83 plays only a structural role in siroheme binding that is coupled to the structure of the flexible active site loop with no role in proton transfer (Table 2 and Figure 6). Not surprisingly, N149 and R153 are critical determinants of the structure of that flexible loop in anion binding and release (Figure 6). Each of the residues we probed plays a specific, nonredundant role in catalysis that we describe below to build an integrated model of enzyme activity.

R83S. In oxidized *E. coli* SiRHP, R83 is positioned such that its planar guanidinium group stacks against a siroheme

dx.doi.org/10.1021/bi300947a | *Biochemistry* 2012, 51, 9857−9868

proponyl that is joined at one of the unconjugated pyrroline rings, B, and also forms hydrogen bonds to O4 of the bound phosphate (Figure 6A). When SO_3^{2-} binds, R83 also interacts with both a substrate oxygen (O2) and the siroheme (Figure 6B). This interaction is maintained in the NO_2^--bound species but breaks when linear molecules are bound.[11]

The R83S variant shows a significant decrease in siroheme occupancy (only 6% of the purified enzyme has siroheme bound) and in stability, measured by its extreme sensitivity to cleavage by trypsin (Table 2 and Figure S1 of the Supporting Information). Further, this siroheme-free R83S variant has a markedly different CD spectrum, indicative of an increase in helical content (Figure S2 and Table S1 of the Supporting Information) and does not bind HPO_4^{2-} (Figure 5). Certainly, this altered CD spectrum and decreased stability need further exploration to improve our understanding of the complex relationship between the protein and its central cofactor. In the context of these assays, however, the cofactor is central to activity so the majority of expressed R83S protein, which lacks siroheme, is not active for SO_3^{2-} reduction.

The small population of R83S protein that is bound with siroheme is somewhat active in reducing SO_3^{2-} despite its substantial siroheme binding defect, its HPO_4^{2-} binding defect, and the instability of the siroheme-free protein (Table 2, Figure 5, and Figure S1 of the Supporting Information). Further, the fraction of this variant that is active produces a fully reduced product with a 6:1 electron:sulfite ratio and is more active in reducing NH_2OH than the wild type (Table 2). The low siroheme occupancy and coupled structural perturbation measured by CD explain this variant's inability to complement the *cysI*$^-$ deficiency in M9 minimal medium despite a near-normal expression level and activity of the small fraction that binds siroheme.

Together, these results suggest that the primary roles of R83 are to anchor the siroheme and the bound HPO_4^{2-} but not to provide protons for catalysis. Although R83 participates in SO_3^{2-} and NO_2^- binding, this interaction is not essential for full turnover or for product release; therefore, R83 is not likely a direct or indirect proton source for oxidative cleavage of the X−O bond. Given that, R83's side chain participates in the general pull mechanism by contributing to the overall positive charge on the siroheme's distal face, and when replaced by serine, the siroheme-bound R83S variant is only ∼60% as active as the wild-type enzyme in reducing SO_3^{2-}.

R153S. In *E. coli* SiRHP, R153 sits at the base of the flexible active site loop that is partially disordered in the resting, HPO_4^{2-}-bound form (Figure 6A). Unique among the other four cage-forming residues, R153 does not interact with the siroheme and changes conformation depending on the bound anion (Figure 6B). In the HPO_4^{2-}-bound form, R153 is flipped away from the active site such that its Nε forms a hydrogen bond with O4 of the HPO_4^{2-}, which is solvent-exposed, whereas its Nη2 forms a hydrogen bond with a solvent-exposed water molecule (Figure 6A).[3] When SO_3^{2-} binds, R153's guanidinium group flips over, creating space for the flexible loop to coalesce around the active site and anchor the bound substrate by positioning Nη1 near the third, solvent-exposed oxygen of SO_3^{2-} (O3). R153 Nη2 maintains its interaction with the solvent-exposed water molecule, which also interacts with substrate O3 (Figure 6B). The O3−S bond is ∼0.3 Å longer (1.62 Å) than the O1−S and O2−S bonds (1.36 and 1.32 Å, respectively) so is proposed to be protonated and the first water released as the electron transfer takes place.[13]

The structure of the R153S variant mimics the SO_3^{2-}-bound native enzyme in the clamped position of the flexible active site loop and in the ordering of the adjacent helix (Figure 6B,C). In this variant, the diffuse shape of the HPO_4^{2-} density (Figure 4) and the anion's high *B* factor suggest that without the R153 hydrogen bond, the bound anion is less tightly coordinated in the distal pocket of the siroheme. Further, weak density and high *B* factors of active site water molecules suggest the solvent molecules are not as well ordered as they are in the wild-type or N149W variant structures (Figure 4). The clamped loop conformation explains the lack of exchange between HPO_4^{2-} and SO_3^{2-} (Figure 5) because the HPO_4^{2-} is trapped within the active site cavity, unable to freely diffuse out.

The R513S variant is partially active for electron transfer (Table 2), suggesting that upon reduction the active site loop does release HPO_4^{2-}, as in the wild type.[13] Despite its residual activity, however, the R153S variant does not complement the *cysI*$^-$ deficiency when grown under selecting conditions (Figure 2). In contrast to R83S, R153S is mostly bound with siroheme and has a native CD spectrum (Table 2 and Table S1 and Figure S2 of the Supporting Information), suggesting a mechanistic, rather than structural, cause for its inability to complement. Indeed, R153S uses four electrons for each atom of sulfur it reduces. This single-amino acid variation interferes significantly with the pull mechanism by removing the source for one of the later proton transfer steps and releasing the partially reduced product in the S^0 state, probably as the SO^- species. Such an intermediate would be unstable and spontaneously react to produce a partially reduced sulfur intermediate that maintains its ability to form methylene blue with DPD and $FeCl_3$-HCl.

K217S. In *E. coli* SiRHP, K217 is an electrostatic anchor, coordinating the siroheme's buried acetyl and proponyl groups from ring C as well as the buried oxygens of HPO_4^{2-}, SO_3^{2-}, NO_2^-, and NO (Figure 6A,B).[11] Not surprisingly, K217S is unable to bind the resting state HPO_4^{2-} (Figure 5). Like R83S, K217S is unable to complement the *cysI*$^-$ deficiency, in part because of its low siroheme occupancy, marked by changes to this variant's CD spectrum (Table 2 and Table S1 and Figure S2 of the Supporting Information). When normalized for the lack of siroheme, K217S shows a reduced level of electron transfer when provided with SO_3^{2-}, only reducing sulfur with 5 electron equivalents per sulfur atom (Table 2). This would release partially reduced intermediates in the S^- state. Like other partially reduced sulfur compounds, this intermediate would not be stable in aqueous solution but would decay into a species that can still form methylene blue with DPD and $FeCl_3$-HCl. In contrast, the K217S variant is quite reactive toward NH_2OH, showing that it is capable of anion binding and rapid proton and electron transfer.

K215S. In *E. coli* SiRHP, K215 interacts with siroheme, coordinating the siroheme's solvent-exposed acetyl group on ring D opposite from the hydrophobic interactions provided by R83, as well as the ordered water molecule at the mouth of the active site (Figure 6A). When HPO_4^{2-} is bound, K215 joins K217 to tightly coordinate the buried O3; as with K217S, K215S is unable to coordinate HPO_4^{2-} in solution (Figure 5).

Like R153S, K215S does not complement the *cysI*$^-$ deficiency, shows a native CD spectrum, and is mostly siroheme-bound (Figure 2 and Tables S1 and S2 of the Supporting Information). HPO_4^{2-} binding is eliminated (Figure 5), but the enzyme shows minimal activity with SO_3^{2-} as a substrate so anion binding is not completely

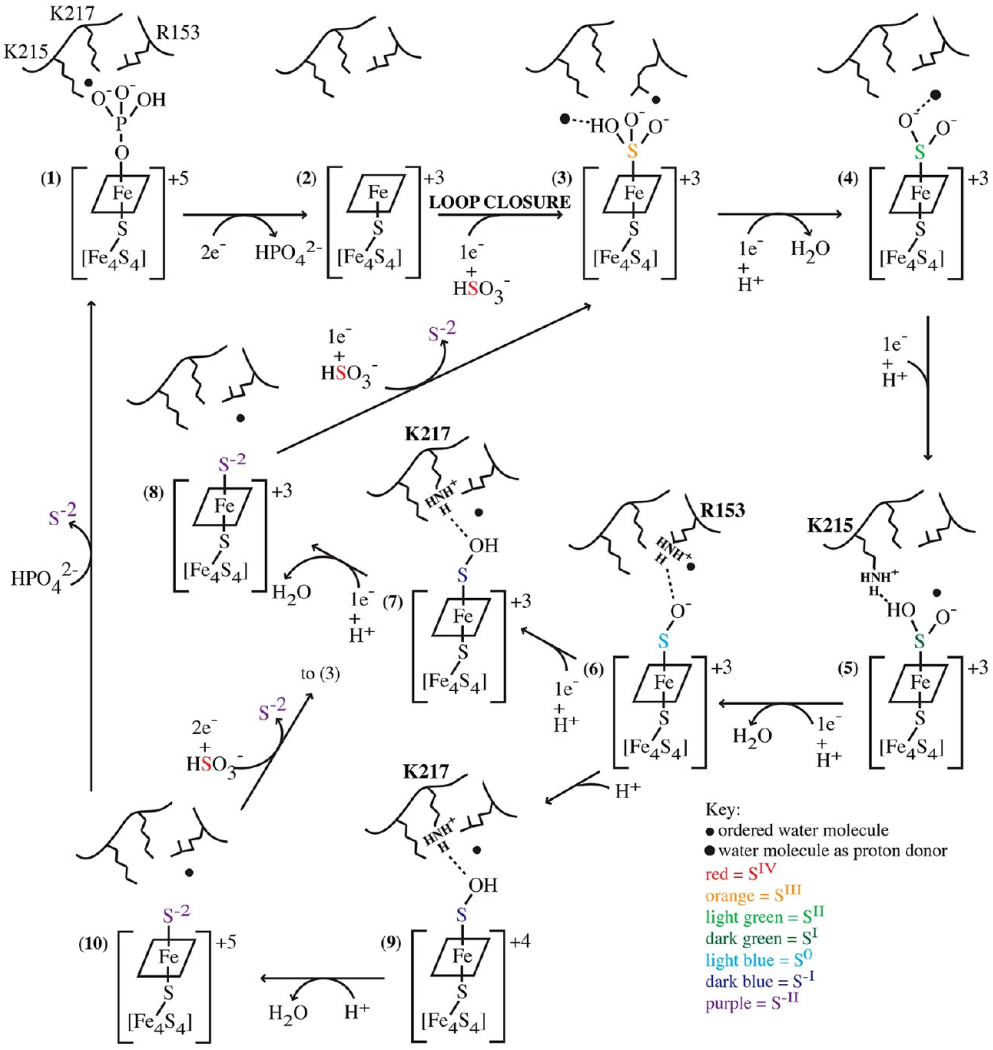

Figure 7. Proposed mechanism for the sequential six-electron reduction of SiRHP based on functional assays of the active site variants R83S, R153S, K215S, and K217S. In this scheme, ordered water molecules are represented by small dots and water molecules that serve as proton donors by larger dots. Each redox state of the sulfur is represented by a different color (see the key in the diagram). The proton donor and substrate oxygen acceptor are linked by a dotted line. By this mechanism, protons and electrons are passed sequentially from the enzyme to the substrate. In step 1 to 2, electrons reduce the system and prime HPO_4^{2-} release. Substrate binds as the protonated HSO_3^- in step 2 to 3 before the first dehydration is catalyzed by the transfer of a proton from an ordered active site water molecule in step 3 to 4. Another proton is supplied from an active site water molecule in step 4 to 5 to prepare for the next dehydration reaction. K215 supplies the next proton, driving the second dehydration reaction from step 5 to 6. Depending on the stoichiometry of the reductant, the path bifurcates but the protons continue to be added sequentially, first from R153 in step 6 to 7/9 and then from K217 in step 7 to 8 or 9 to 10, as the final dehydration reaction occurs. HPO_4^{2-} or SO_3^{2-} rebinds, completing the cycle.

abrogated (Table 2). K215S uses ~3 electrons per molecule of reduced sulfur (Table 2), again highlighting the related electron push−pull mechanism. Further, the fact that K217S and K215S can both release partially reduced sulfur equivalents with an odd number of electron equivalents supports the hypothesis that electrons can move one at a time, a property first observed using EPR to trap the ferroheme−NO intermediate.[15] At this intermediate stage of reduction, K125S releases sulfur in an S^+ state, probably as HSO_2^-, another unstable intermediate that would decay into a species capable of forming methylene blue with DPD and $FeCl_3$.

N149W. One important feature of SiRHP anion binding is the flexible loop that contains N149 and coalesces around the active site upon SO_3^{2-} binding, coupled to R153 reorganization (Figure 6A,B). This same loop is seen covering access to the active site in *af*DSR's structural siroheme site, and the analogous residue, a tryptophan, projects into the active site (Figure 1A).[5] To test the effect of having a large, bulky residue on this loop, we created the N149W variation in SiRHP that highlights the link among the flexible active site loop, SiRHP's N-terminus, and reactivity.

Unlike in the structure of the *af*DSR enzyme, W149 does not project into the active site (Figure 6D). Although N149W is sensitive to trypsin cleavage (Figure S1 of the Supporting Information), the CD spectrum of full-length N149W is the same as that of the wild-type enzyme (Figure S2 of the Supporting Information) so the mutation does not cause global unfolding. Further, the position of the loop amino acids can be determined from the X-ray crystallographic analysis (Figure 3A). From that analysis, we also know that adding the bulky side chain in the active site loop at this position causes the N-terminus to bifurcate. One path follows the same trajectory as

dx.doi.org/10.1021/bi300947a | *Biochemistry* 2012, 51, 9857−9868

in the wild-type enzyme. In the other, the backbone of L81, L82, and R83 shifts in position toward this more open loop, giving R83 enough space to flip over and, perhaps, enhancing the tendency of the N-terminus to be cleaved by trypsin. In this new position, R83 Cβ and Leu145 Cβ come ~3.1 Å closer, within ~4.1 Å of one another. Further, R83 Cγ and R153 Cγ come ~1.3 Å closer to one another, within 4.3 Å of one another. In this way, R83 acts like a hydrophobic prop to keep the active site loop open. The N149W structure shows that the flexibility in this loop can accommodate the bulky side chain (Figure 6D), so its presence on that loop is not the sole determinant of the *af*DSR subunit's lack of reactivity.

N149W does not release bound HPO_4^{2-} in the slow exchange with SO_3^{2-} like the wild-type enzyme does under oxidizing conditions in the presence of excess HPO_4^{2-} (Figure 5). Under anaerobic conditions and in the absence of HPO_4^{2-}, however, SO_3^{2-} binds to the active site of N149W, and we were able to determine the structure of this variant in the presence of the substrate (Table 1). In the N149W variant SO_3^{2-}-bound structure, R153 flips over to interact with SO_3^{2-} as it does in the wild-type enzyme, but the active site loop does not coalesce (Figure 6B,E). Taken together, these observations suggest that the lack of anion exchange in the presence of excess HPO_4^{2-} may be caused by tighter HPO_4^{2-} binding due to the repositioned R83 side chain (Figure 6D), weaker SO_3^{2-} binding because of the open position of the active site loop because of the bulky N149W addition (Figure 6E), or a combination of the two anion binding defects.

Wild-type SiRHP reacts with NO_2^- with a higher V_{max}, but a higher K_m, than it does with SO_3^{2-}.[17] Further, the active site loop does not coalesce when NO_2^- binds the siroheme.[11] The clamping of the substrate loop has, therefore, been proposed to explain the specificity of SiRHP for its endogenous substrate by increasing the binding affinity of, rather than catalytic rate of, the enzyme for SO_3^{2-}.[11] Despite structural changes, the N149W variant is more active in reducing SO_3^{2-} than wild-type SiRHP, both measured by complementation (Figure 2) and reactivity with SO_3^{2-} and NH_2OH (Table 2). This enhanced reactivity of the N149W variant with SO_3^{2-} relative to that of the wild-type enzyme and the disorder in the active site loop upon SO_3^{2-} binding are analogous to the reactivity of the wild-type enzyme with NO_2^-. In both cases, the enzyme acts with a higher V_{max} when the active site loop does not move to clamp over the bound anion, supporting the hypothesis that loop closure during SO_3^{2-} turnover may be rate-limiting.

The Detailed Mechanism for SiRHP Includes Sequential, Single-Electron and -Proton Transfer. Taken together, these results suggest an important, refined mechanism for SiRHP activity by showing that SiRHP can transfer electrons sequentially and by identifying the proton donors at each step (Figure 7). In total, six electrons and six protons move from the protein environment onto the substrate. For initial substrate binding to occur in a rapid fashion, the enzyme cofactors are doubly reduced from +5 to +3 and HPO_4^{2-} diffuses from the siroheme's distal binding site (Figure 7, step 1 to 2).[13,26] Substrate does not bind to the oxidized enzyme because the active site is blocked by the presence of HPO_4^{2-} (Figure 6A), but there is no overall change in the active site structure upon HPO_4^{2-} release, other than the lack of ordered active site solvent (PDB entries 1AOP and 5AOP, respectively).[3,13] In the assimilatory enzyme, the electrons come from the SiR flavoprotein subunit (SiRFP) that has two flavin cofactors and a diffusible NADPH.[27] In the isolated SiRHP that we studied here, the electrons come from a chemical reductant, MV^+.

The first proton comes into the active site as HSO_3^-, shown by the lengthened S−OH bond seen in native HSO_3^--bound SiRHP as the loop closes down (Figure 6B and Figure 7, step 2 to 3; PDB entries 5AOP and 2GEP, respectively).[11] As in the wild-type enzyme, R153 is repositioned upon HSO_3^- binding in the N149W variant (Figure 6B,E). Unlike that of the wild-type enzyme, the active site loop in this variant does not draw down with addition of the bulky side chain at position 149, suggesting that the repositioning of the long arginine side chain is not sufficient for loop closure (Figure 6B,E). Concomitant with protonated substrate binding, the first electron is likely pushed onto the substrate by the prereduced cofactors,[28] priming the first dehydration reaction (Figure 7, step 3, PDB entry 2GEP[11]). Importantly, EPR studies of the SO_3^{2-}-bound enzyme yields ambiguous results about the redox state of the steady state cofactors, whereas a three-electron reduced intermediate bearing a ferroheme−NO complex has been identified when NO_2^- is the acceptor,[15] demonstrating the plausibility of the single-electron transfer in this system.

An ordered water molecule present in the mouth of the active site of the substrate-bound enzyme (Figure 6B,E, labeled in red) is the likely candidate for the proton donor that helps pull the second electron from the cofactors, catalyzing the first dehydration without direct participation by any active site side chain (Figure 7, step 3 to 4; PDB entries 2GEP and 3GEO, respectively[11]). The hypothesis that the first proton comes in on the protonated substrate and the second proton is supplied by an ordered water molecule is further supported by our observation that each point variant, except K215S, can rapidly and efficiently reduce NH_2OH, which needs only two electrons and two protons to generate NH_3 (Table 2). K215 is critical for binding the anion throughout the cycle,[11] so its reduced activity can be understood in terms of a binding defect.

At this point, two protons and two electrons have been used, with the release of one water molecule leaving behind the trigonal planar SO_2^{2-} (Figure 7, step 4; PDB entry 3GEO). SO_2^{2-} is an unstable intermediate, but NO_2^- is an alternative substrate and binds to SiRHP without R153 reorganization or loop closure.[11] A single water molecule remains deep in the active site, whereas K215 Nζ make the closest contact with the buried substrate oxygen.[11] The second proton donor is likely that buried water molecule, and with its transfer, a third electron comes from the cofactors onto the substrate to be replaced by SiRFP or the chemical reductant (Figure 7, step 4 to 5; PDB entry 3GEO).

No water molecule is released from the substrate until the transfer of a fourth proton from K215 (either directly or indirectly through an ordered water molecule) helps pull another electron onto the substrate, catalyzing the second dehydration (Figure 7, step 5 to 6; PDB entries 3GEO and 6GEP, respectively[11]). K215 is appropriately positioned for this role between the mouth of the active site and the buried substrate oxygen, making contact with the oxygen of the longer N−O bond in the NO_2^--bound wild-type structure.[11] Further, the K215S variant uses three electrons for each reduced sulfur equivalent that it releases (Table 2), suggesting that the reaction stalls out before the fourth proton−electron pair can move.

The second dehydration reaction leaves behind the unstable SO^- intermediate bound to the siroheme (Figure 7, step 6; PDB entry 6GEP[11]). NO also binds the active site, mimicking

binding of this linear molecule and flipping R153S to make a hydrogen bond with the substrate oxygen; a buried water molecule also interacts with the substrate oxygen and R153.[11] Thus positioned, R153 provides the fifth proton, either directly or through that ordered water molecule, while another electron moves onto the sulfur atom (Figure 7, step 6 to 7/9; PDB entries 6GEP and 7GEP, respectively[11]). Bifurcation of the reaction cycle occurs here because the reaction pathway depends on the stoichiometry of electrons available to the enzyme.

At this stage, the final two electrons are stored on the cofactors. In the presence of excess reductant, the reaction could continue moving electrons one at a time through the coupled cofactors while the reducing equivalents are replaced by either SiRFP or a chemical reductant (Figure 7, step 6 to 7). In a limiting level of reductant, the transfer of an electron to the cofactors would be complete and the two remaining electrons would come sequentially off each of the metal cofactors (Figure 7, step 6 to 9). Regardless, the hypothesis that R153 is responsible for the fifth proton transfer is supported by the favorable geometry of the active site with a bound linear anion[11] and the observation that the R153S variant uses four electrons for each reduced sulfur equivalent that it releases (Table 2), suggesting that the reaction stalls out before the transfer of the fifth electron. Proton transfer in the wild-type enzyme leaves behind the protonated, unstable intermediate SOH.

Finally, K217 provides the sixth and final proton, either directly or indirectly through an active site water molecule, to pull the last electron onto the substrate and catalyze the third dehydration (Figure 7, step 7 to 8 or step 9 to 10). K217 is the most buried of the side chains, serves as an anchor for all the other anionic species as they undergo serial dehydration, and makes a long hydrogen bond with the oxygen of the partially reduced S−X anion, the closest structure representing step 7 to 9 (PDB entry 7GEP).[11] This hypothesis is further supported by the observation that K217S uses five electrons for each reduced sulfur equivalent that it releases, stopping before the final product can be released (Table 2). After this final electron and proton transfer and water and product release, another substrate molecule could bind along with the appropriate reducing equivalents to continue the cycle (step 8 to 3 or step 10 to 3) or the enzyme could return to its resting, oxidized state with phosphate bound in the distal siroheme pocket (step 10 to 1).

Summary. Our results reveal intricate details about how SiRHP moves six electrons to a siroheme-bound anion in a unique, complex redox reaction that couples anion binding, conformational changes, electron transfer, and proton transfer. By removing putative proton donors through point mutation, we have identified the source from which, and order in which, each proton is provided to drive catalysis. The first three protons come from solvent, either as part of the HSO_3^- anion or from ordered active site waters. The last three come from K215, R153, and K217. By characterizing the anion binding ability of variations to those residues, coupled to structural analysis, we have also elucidated the role of the active site loop in anion binding and release. This new insight into the mechanism of assimilatory SiRHP explains the decades-old observation that SiRHP can achieve a three-electron reduced intermediate along the pathway of NO_2^- reduction and provides a new understanding of "large-volume" electron transfer reactions from coupled metallic cofactors.

■ ASSOCIATED CONTENT

Ⓢ Supporting Information

Details about the trypsin stability, circular dichroism and cofactor refinement experiments. This material is available free of charge via the Internet at http://pubs.acs.org.

Accession Codes

Coordinates for N149W (entry 4G38), N149W-SO_3^{2-} (entry 4HTR), and R153S (entry 4G39) have been deposited in the Protein Data Bank.

■ AUTHOR INFORMATION

Corresponding Author

*Address: 91 Chieftan Way, Tallahassee, FL 32306-4380. Phone: (850) 645-9318. E-mail: mestroupe@bio.fsu.edu.

Funding

This work was supported by National Science Foundation Grant 1149763 to M.E.S.

Notes

The authors declare no competing financial interest.

■ ACKNOWLEDGMENTS

Thanks to Drs. Brian Miller, Betty Gaffney, and Christopher Stroupe for helpful discussion, Dr. Mykhailo Shatruk for use of his anaerobic glovebox and spectrophotometer, Dr. Claudius Mundoma for assistance with the CD experiments, and Nigel Moriarty for help with the siroheme restraints in PHENIX. X-ray crystallographic data were collected at the Southeast Regional Collaborative Access Team (SER-CAT) 22-ID (or 22-BM) beamline at the Advanced Photon Source, Argonne National Laboratory. Supporting institutions may be found at http://www.ser-cat.org/members.html. Use of the Advanced Photon Source was supported by the U.S. Department of Energy, Office of Science, Office of Basic Energy Sciences, under Contract W-31-109-Eng-38. Molecular graphics were created and analyses performed with the UCSF Chimera package. Chimera is developed by the Resource for Biocomputing, Visualization, and Informatics at the University of California, San Francisco, with support from the National Institutes of Health (National Center for Research Resources Grant 2P41RR001081 and National Institute of General Medical Sciences Grant 9P41GM103311).

■ ABBREVIATIONS

SiRHP, sulfite reductase hemoprotein; SO_3^{2-}, sulfite; S^{2-}, sulfide; NO_2^-, nitrite; NH_3, ammonia; DSR, dissimilatory sulfite reductase; KP_i, potassium phosphate buffer; K_2HPO_4, potassium phosphate; LB, Luria-Bertani; BCA, bichinoic acid; SDS−PAGE, sodium dodecyl sulfate−polyacrylamide gel electrophoresis; MV^+, methyl viologen; NH_2OH, hydroxylamine; DPD, *N*,*N*-dimethyl-*p*-phenylenediamine; CD, circular dichrosim; SiRFP, sulfite reductase flavoprotein; PDB, Protein Data Bank.

■ REFERENCES

(1) Sekowska, A., Kung, H. F., and Danchin, A. (2000) Sulfur metabolism in *Escherichia coli* and related bacteria: Facts and fiction. *J. Mol. Microbiol. Biotechnol. 2*, 145−177.

(2) Rabus, R., Hansen, T. A., and Widdel, F. (2006) Dissimilatory Sulfate- and Sulfur-Reducing Prokaryotes. In *The Prokaryotes: Ecophysiology and Biochemistry* (Dworkin, M., Falkow, S., Rosenberg, E., Schleifer, K., and Stackebrandt, E., Eds.) pp 659−768, Springer, New York.

(3) Crane, B. R., Siegel, L. M., and Getzoff, E. D. (1995) Sulfite reductase structure at 1.6 Å: Evolution and catalysis for reduction of inorganic anions. *Science 270*, 59−67.
(4) Schnell, R., Sandalova, T., Hellman, U., Lindqvist, Y., and Schneider, G. (2005) Siroheme- and [Fe_4-S_4]-dependent NirA from *Mycobacterium tuberculosis* is a sulfite reductase with a covalent Cys-Tyr bond in the active site. *J. Biol. Chem. 280*, 27319−27328.
(5) Schiffer, A., Parey, K., Warkentin, E., Diederichs, K., Huber, H., Stetter, K. O., Kroneck, P. M., and Ermler, U. (2008) Structure of the dissimilatory sulfite reductase from the hyperthermophilic archaeon *Archaeoglobus fulgidus*. *J. Mol. Biol. 379*, 1063−1074.
(6) Oliveira, T. F., Vonrhein, C., Matias, P. M., Venceslau, S. S., Pereira, I. A., and Archer, M. (2008) The crystal structure of *Desulfovibrio vulgaris* dissimilatory sulfite reductase bound to DsrC provides novel insights into the mechanism of sulfate respiration. *J. Biol. Chem. 283*, 34141−34149.
(7) Hsieh, Y. C., Liu, M. Y., Wang, V. C., Chiang, Y. L., Liu, E. H., Wu, W. G., Chan, S. I., and Chen, C. J. (2010) Structural insights into the enzyme catalysis from comparison of three forms of dissimilatory sulphite reductase from *Desulfovibrio gigas*. *Mol. Microbiol. 78*, 1101−1116.
(8) Fritz, G., Roth, A., Schiffer, A., Buchert, T., Bourenkov, G., Bartunik, H. D., Huber, H., Stetter, K. O., Kroneck, P. M., and Ermler, U. (2002) Structure of adenylylsulfate reductase from the hyperthermophilic *Archaeoglobus fulgidus* at 1.6-Å resolution. *Proc. Natl. Acad. Sci. U.S.A. 99*, 1836−1841.
(9) Stroupe, M. E., and Getzoff, E. D. (2005) The role of siroheme in sulfite and nitrite reductases. In *Tetrapyrroles: Their birth, life, and death* (Warren, M. J., and Smith, A., Eds.) Landes Bioscience, Georgetown, TX.
(10) Murphy, M. J., and Siegel, L. M. (1973) Siroheme and sirohydrochlorin. The basis for a new type of porphyrin-related prosthetic group common to both assimilatory and dissimilatory sulfite reductases. *J. Biol. Chem. 248*, 6911−6919.
(11) Crane, B. R., Siegel, L. M., and Getzoff, E. D. (1997) Probing the catalytic mechanism of sulfite reductase by X-ray crystallography: Structures of the *Escherichia coli* hemoprotein in complex with substrates, inhibitors, intermediates, and products. *Biochemistry 36*, 12120−12137.
(12) Parey, K., Warkentin, E., Kroneck, P. M., and Ermler, U. (2010) Reaction cycle of the dissimilatory sulfite reductase from *Archaeoglobus fulgidus*. *Biochemistry 49*, 8912−8921.
(13) Crane, B. R., Siegel, L. M., and Getzoff, E. D. (1997) Structures of the siroheme- and Fe_4S_4-containing active center of sulfite reductase in different states of oxidation: Heme activation via reduction-gated exogenous ligand exchange. *Biochemistry 36*, 12101−12119.
(14) Schlegel, B. P., Jez, J. M., and Penning, T. M. (1998) Mutagenesis of 3α-hydroxysteroid dehydrogenase reveals a "push-pull" mechanism for proton transfer in aldo-keto reductases. *Biochemistry 37*, 3538−3548.
(15) Janick, P. A., Rueger, D. C., Krueger, R. J., Barber, M. J., and Siegel, L. M. (1983) Characterization of complexes between *Escherichia coli* sulfite reductase hemoprotein subunit and its substrates sulfite and nitrite. *Biochemistry 22*, 396−408.
(16) Wu, J. Y., Siegel, L. M., and Kredich, N. M. (1991) High-level expression of *Escherichia coli* NADPH-sulfite reductase: Requirement for a cloned *cysG* plasmid to overcome limiting siroheme cofactor. *J. Bacteriol. 173*, 325−333.
(17) Siegel, L. M., Rueger, D. C., Barber, M. J., Krueger, R. J., Orme-Johnson, N. R., and Orme-Johnson, W. H. (1982) *Escherichia coli* sulfite reductase hemoprotein subunit. Prosthetic groups, catalytic parameters, and ligand complexes. *J. Biol. Chem. 257*, 6343−6350.
(18) Baba, T., Ara, T., Hasegawa, M., Takai, Y., Okumura, Y., Baba, M., Datsenko, K. A., Tomita, M., Wanner, B. L., and Mori, H. (2006) Construction of *Escherichia coli* K-12 in-frame, single-gene knockout mutants: The Keio collection. *Mol. Syst. Biol. 2*, 0008.
(19) Sambrook, J., Fritsch, E. F., and Maniatis, T. (1989) *Molecular Cloning: A Laboratory Manual*, 2nd ed., Vol. 3, Cold Spring Harbor Laboratory Press, Plainview, NJ.
(20) Otwinowski, Z., and Minor, W. (1997) Processing of X-ray Diffraction Data Collected in Oscillation Mode. *Methods Enzymol. 276*, 307−326.
(21) Adams, P. D., Afonine, P. V., Bunkoczi, G., Chen, V. B., Davis, I. W., Echols, N., Headd, J. J., Hung, L. W., Kapral, G. J., Grosse-Kunstleve, R. W., McCoy, A. J., Moriarty, N. W., Oeffner, R., Read, R. J., Richardson, D. C., Richardson, J. S., Terwilliger, T. C., and Zwart, P. H. (2010) PHENIX: A comprehensive Python-based system for macromolecular structure solution. *Acta Crystallogr. D66*, 213−221.
(22) Emsley, P., Lohkamp, B., Scott, W. G., and Cowtan, K. (2010) Features and development of Coot. *Acta Crystallogr. D66*, 486−501.
(23) Thorneley, R. N. (1974) A convenient electrochemical preparation of reduced methyl viologen and a kinetic study of the reaction with oxygen using an anaerobic stopped-flow apparatus. *Biochim. Biophys. Acta 333*, 487−496.
(24) Siegel, L. M. (1965) A Direct Microdetermination for Sulfide. *Anal. Biochem. 11*, 126−132.
(25) Read, R. J. (1986) Imporved Fourier coefficients for maps using phases from partial structures with errors. *Acta Crystallogr. A42*, 140−149.
(26) Murphy, M. J., Siegel, L. M., and Kamin, H. (1974) Reduced nicotinamide adenine dinucleotide phosphate-sulfite reductase of enterobacteria. VI. The reaction of carbon monoxide with the *Escherichia coli* holoenzyme, the hemoprotein, and free siroheme. *J. Biol. Chem. 249*, 1610−1614.
(27) Siegel, L. M., Davis, P. S., and Kamin, H. (1974) Reduced nicotinamide adenine dinucleotide phosphate-sulfite reductase of enterobacteria. 3. The *Escherichia coli* hemoflavoprotein: Catalytic parameters and the sequence of electron flow. *J. Biol. Chem. 249*, 1572−1586.
(28) Janick, P. A., and Siegel, L. M. (1983) Electron paramagnetic resonance and optical evidence for interaction between siroheme and Fe_4S_4 prosthetic groups in complexes of *Escherichia coli* sulfite reductase hemoprotein with added ligands. *Biochemistry 22*, 504−515.
(29) Pettersen, E. F., Goddard, T. D., Huang, C. C., Couch, G. S., Greenblatt, D. M., Meng, E. C., and Ferrin, T. E. (2004) UCSF Chimera: A visualization system for exploratory research and analysis. *J. Comput. Chem. 25*, 1605−1612.